Acta Crystallographica Section A
Foundations of Crystallography
ISSN 0108-7673

Received 3 March 2010
Accepted 19 March 2010

High-resolution study of dynamical diffraction phenomena accompanying the Renninger (222/113) case of three-beam diffraction in silicon

A. Kazimirov[a]* and V. G. Kohn[b]

[a]Cornell High Energy Synchrotron Source (CHESS), Cornell University, Ithaca, 14853 NY, USA, and [b]Russian Research Center 'Kurchatov Institute', 123182 Moscow, Russia. Correspondence e-mail: ayk7@cornell.edu

X-ray optical schemes capable of producing a highly monochromatic beam with high angular collimation in both the vertical and horizontal planes have been evaluated and utilized to study high-resolution diffraction phenomena in the Renninger (222/113) case of three-beam diffraction in silicon. The effect of the total reflection of the incident beam into the nearly forbidden reflected beam was observed for the first time with the maximum 222 reflectivity at the 70% level. We have demonstrated that the width of the 222 reflection can be varied many times by tuning the azimuthal angle by only a few μrad in the vicinity of the three-beam diffraction region. This effect, predicted theoretically more than 20 years ago, is explained by the enhancement of the 222 scattering amplitude due to the virtual two-stage 000 → 113 → 222 process which depends on the azimuthal angle.

1. Introduction

The general theory of *n*-beam diffraction is based on the assumption that the incident beam is a perfect plane monochromatic wave and the theory describes the wavefield in a crystal as a superposition of *n* plane waves. To compare theory with experiment the resulting intensities are integrated over the finite angular spread on the incident beam (Colella, 1974). While this is sufficient for the analysis of the effects related to the phases of the reflections involved in multiple diffraction (which is one of the main established application areas for multiple diffraction), any high-resolution dynamical phenomena taking place within a narrow angular range of a few Darwin widths for a particular reflection are washed out and lost from the analysis.

In non-coplanar multiple X-ray diffraction, the diffraction conditions are usually defined by two angles, a polar angle θ and an azimuthal angle φ. In a typical experiment at synchrotron sources the primary scattering plane is vertical, the polar angle is associated with the rotation around the horizontal axis perpendicular to this plane and the azimuthal angle is associated with the rotation around the axis lying in the vertical plane. Thus, for a well known Renninger scheme the θ angle corresponds to the Bragg angle for the forbidden 222 reflection and the φ angle describes the rotation around the normal to the crystal surface.

In spite of a great number of theoretical and experimental works on multiple diffraction, including the Renninger effect, published so far (see Chang, 2004; Authier, 2005 and references therein), there are very few experimental works in which dynamical diffraction effects accompanying multiple diffraction have been studied with sufficiently high resolution. Indeed, to observe these effects one needs to condition the incident X-ray beam to a degree approaching a perfect plane wave. That requires a two-dimensional angular collimation and a high degree of monochromatization. The excitation of the X-ray standing wavefields in three-beam (111/220) diffraction was studied by Kazimirov *et al.* (1992) and Kazimirov, Kovalchuk, Kohn, Kharitonov *et al.* (1993). In these works, a two-dimensional angular collimation was achieved by using another interesting dynamical diffraction effect – the effect of the enhancement of the anomalous transmission (super-Borrmann effect) in a six-beam symmetrical Laue diffraction (Afanas'ev & Kohn, 1977). In the work by Kazimirov, Kovalchuk, Kohn, Ishikawa *et al.* (1993) this effect was experimentally measured and compared with theory. Pahl (1994) proposed a novel ultra-small-angle scattering camera based on a super-Borrmann effect, and its feasibility was experimentally verified. The idea of using the Renninger effect for a two-dimensional collimation was proposed by Colella (1974) and analyzed later in both Bragg and Laue cases by Stepanov *et al.* (1994), theoretically and experimentally.

Most of the multiple diffraction experiments were performed at second-generation synchrotron radiation (SR) sources. The beams produced by modern third-generation SR sources, due to a very high intensity and a high degree of the 'natural' angular collimation of undulator radiation, can be more easily conditioned in terms of both a two-dimensional angular collimation and a monochromatization. Next-

generation sources such as X-ray free electron lasers (XFELs) and energy-recovery linacs (ERLs) will be able to produce almost perfect plane-wave X-ray beams. These new experimental opportunities provide strong motivations to continue the study of multiple diffraction effects and their potential applications in X-ray optics.

In this article we present the high-resolution study of dynamical diffraction phenomena accompanying the Renninger Si (222/113) case of three-beam diffraction. First experimental rocking-curve measurements at the exact (222/113) excitation in Ge were performed by Colella (1974) using a double-crystal setup in the antiparallel arrangement. Much better collimation than that provided by a double-crystal setup is required in both directions to observe the details of the dynamical diffraction interaction. In particular, the goal of this work was to observe the effect of a total reflection of a parallel incident beam into the forbidden 222 reflected beam predicted by Kohn (1988). This effect takes place in a very narrow polar angular range and rather wide azimuthal angular range near the three-beam diffraction region where the 113 reflection is very small. It has never been observed experimentally because of the difficulty of preparing an incident beam approaching a perfect plane wave. This work presents such attempts. We studied five optical setups that provide various degrees of monochromatization and angular collimation in both the vertical and horizontal planes. For each of these optics we measured the 222 and 113 diffraction curves in the vicinity of the three-beam (222/113) diffraction region. For our best optics we recorded 68% reflectivity of the 222 reflected beam. We observed experimentally a remarkable phenomenon: the width of the 222 strong reflection region can be changed many times (about four times in our setup) by tuning the azimuthal angle by a few μrad while still at the 60% reflectivity level. In §2 the theoretical description of the excitation of the forbidden reflection is presented. Then we present the experimental results followed by the discussion and conclusions.

2. Theory

The general theory of plane-wave multiple diffraction in a single crystal is well developed (Colella, 1974; Kohn, 1979; Chang, 2004). In this section, we formulate the theoretical approach which has been effectively utilized for computer simulations. The normalized reflection powers for the beams which leave the crystal through the entrance surface can be calculated by means of the formula

$$R_m^{(s)}(\theta,\varphi)=\sum_{s'}\left|\sum_j B_{ms'}(j)c_s(j)\right|^2, \tag{1}$$

where the index m is used for the beams ($m=0$ for the incident beam), $s, s'=\pi,\sigma$ indicate the polarization state of the electric field vector of the beams, the index j allows one to distinguish various Bloch waves or zones of dispersion surface, and the parameters $c_s(j)$ determine the rate of excitation of the jth Bloch wave. The summation is performed over the values which correspond to the positive value of the absorption coefficent $\mu_j=\Im(\varepsilon_j)$. The Bloch-wave amplitudes $B_{ms}(j)$ and the dispersion parameters ε_j are the solution of the eigenvalue problem

$$\sum_{ns'} G_{mn}^{ss'}(\theta,\varphi)B_{ns'}(j)=\varepsilon_j B_{ms}(j), \tag{2}$$

where the scattering matrix G is determined as

$$G_{mn}^{ss'}(\theta,\varphi)=\frac{2\pi\chi_{mn}}{\lambda\gamma_m^{1/2}\gamma_n^{1/2}}(\mathbf{e}_{ms}\mathbf{e}_{ns'})-\alpha_m(\theta,\varphi)\delta_{mn}^{ss'}. \tag{3}$$

Here $\mathbf{e}_{ms}$ are the unit polarization vectors, λ is the wavelength of X-ray radiation, γ_m is the cosine of the angle between the direction of the mth beam and the internal normal to the entrance surface, χ_{mn} is the Fourier image of the complex polarizability of the crystal with the reciprocal-lattice vector $\mathbf{h}_m-\mathbf{h}_n$, $\delta_{mn}^{ss'}$ is the Kroneker's symbol,

$$\alpha_m(\theta,\varphi)=\frac{2}{\gamma_m}[(\mathbf{h}_m\mathbf{e}_1)\Delta\theta+(\mathbf{h}_m\mathbf{e}_2)\Delta\varphi-(\mathbf{h}_m\mathbf{s}_0)(\Delta\lambda/\lambda)], \tag{4}$$

where $\Delta\theta=\theta-\theta_B$ and $\Delta\varphi=\varphi-\varphi_0$ mean the angular deviation of the incident-beam direction from the direction of kinematically exact multiple diffraction. The unit vectors $\mathbf{e}_1$ and $\mathbf{e}_2$ are normal to the incident-beam direction $\mathbf{s}_0$. We choose $\mathbf{e}_1$ to be in the scattering plane for the forbidden reflection ($m=1$), so $\mathbf{e}_2$ is normal to this plane.

It is known (Kohn, 1979) that in a thick crystal the parameters $c_s(j)=0$ if j indicates the Bloch wave with $\mu_j<0$. The remaining values may be found from the linear set of equations

$$\sum_j B_{ms'}(j)c_{s'}(j)=\delta_{m0}^{ss'}, \tag{5}$$

where the index m runs only over the Laue beams with $\gamma_m>0$. If all the diffracted beams are the Bragg-diffracted beams with $\gamma_m<0$ the situation becomes simpler and we have $c_s(j)=1/B_{0s}(j)$. Equations (1), (2), (3), (4) and (5) allow one to calculate numerically the angular dependence of the reflection power for the diffracted beams. We are interested mainly in the first beam ($m=1$) which we will treat as a pure forbidden. To illustrate the phenomena analytically we simplify the problem and consider hard enough radiation so that the Bragg angles are small which is, in fact, close to our experimental conditions. In this case, one can choose the polarization vectors in such a way that all π vectors are approximately parallel to each other, all σ vectors are also approximately parallel to each other, but all π vectors are normal to the σ vectors. Then, the general sixfold system can be divided into two threefold systems of equations and the index s can be omitted.

Taking into account that $G_{10}=0$ we have for the amplitude of the forbidden beam in the three-beam case

$$B_1=\frac{G_{12}B_2}{(\varepsilon-G_{11})}. \tag{6}$$

As we see from this equation, the forbidden beam can be excited by the beam B_2 and there are two mechanisms for this excitation. The first one corresponds to the large value of B_2 in the angular region where the value of $(\varepsilon-G_{11})$ is not too

large. In this region the forbidden beam is pumped by another strong reflection, so this is the case of a double reflection ($0 \rightarrow 2 \rightarrow 1$). This excitation is realized in the angular region of the multiple diffraction which satisfies the two-beam diffraction condition for beam 2. The second type of excitation takes place if the denominator is small, *i.e.* $(\varepsilon - G_{11}) \simeq 0$. This corresponds to the angular region of the two-beam Bragg condition for the forbidden beam. Now the significant value of B_1 can be obtained even for a small value of B_2. This case can be called a virtual Bragg diffraction, or a resonance diffraction. Indeed, the value B_2 may be small but the amplitude is strongly enhanced by a small value of the resonance denominator.

Let us consider this case in more detail. We have strong B_0 and B_1 amplitudes but a small B_2 amplitude. Also we have small $\Delta\theta$ and rather large $\Delta\varphi$. The amplitude B_2 can be calculated by means of the perturbation method from the system [equation (2)] as

$$B_2 = \frac{G_{20}B_0 + G_{21}B_1}{[\varepsilon - G_{22}(\Delta\varphi)]}. \tag{7}$$

Substitution of this equation into equations for B_0 and B_1 leads to the system

$$g_{00}B_0 + g_{01}B_1 = \varepsilon B_0, \tag{8}$$

$$g_{10}B_0 + g_{11}B_1 = \varepsilon B_1. \tag{9}$$

This system of equations describes a two-beam diffraction with the reflection of the incident beam B_0 into the forbidden beam B_1. The matrix of this system is

$$g_{mn} = G_{mn} + \frac{G_{m2}G_{2n}}{[\varepsilon - G_{22}(\Delta\varphi)]}, \quad m, n = 0, 1. \tag{10}$$

Since these equations are written for the case of a large value of $\Delta\varphi$ and we consider small values of ε, we can replace the denominator by the value $\alpha_2(\Delta\varphi) = [2(\mathbf{h}_2\mathbf{e}_2)/\gamma_2]\Delta\varphi$. Equations (9) and (10), in a more general case and with taking into account polarizations, were obtained for the first time by Høier & Marthinsen (1983) as a method of approximate numerical solution of the multiple diffraction problem. However, we can perform the numerical solution accurately.

Thus, we obtained the case of a two-beam diffraction with a nonzero diffraction parameter for the forbidden beam. It is easy to calculate the solution analytically assuming a symmetrical case ($\gamma_1 = -\gamma_0$) and a pure forbidden first reflection ($\chi_{01} = 0$),

$$\varepsilon = g_{00} + (-g_{01}g_{10})^{1/2}[-y \pm (y^2 - 1)^{1/2}], \tag{11}$$

where

$$y = \frac{g_{00} - g_{11}}{2(-g_{01}g_{10})^{1/2}} = \frac{\Delta\theta\sin(2\theta_B) - X_0}{X_1}, \tag{12}$$

$$X_0 \simeq -\left(\chi_0 + \frac{D_0}{\Delta\varphi}\right), \quad D_0 = \frac{\chi_{02}\chi_{20} - \chi_{12}\chi_{21}}{(\lambda/\pi)(\mathbf{h}_2\mathbf{e}_2)}, \tag{13}$$

$$X_1 \simeq \frac{D_1}{|\Delta\varphi|}, \quad D_1 = \frac{(\chi_{02}\chi_{20}\chi_{12}\chi_{21})^{1/2}}{(\lambda/\pi)|\mathbf{h}_2\mathbf{e}_2|}. \tag{14}$$

The angular dependence of the reflection power to the forbidden beam is determined as

$$R_1 = \left|\frac{B_1}{B_0}\right|^2 = M\widetilde{R}_1, \tag{15}$$

where

$$M = \left|\frac{g_{10}}{g_{01}}\right| = \left|\frac{\chi_{12}\chi_{20}}{\chi_{02}\chi_{21}}\right|, \tag{16}$$

$$\widetilde{R}_1 = \left|-y + (y^2 - 1)^{1/2}\right|^2. \tag{17}$$

Here the square root should be taken with the positive imaginary part. It can be verified straightforwardly that

$$\widetilde{R}_1 = Y - (Y^2 - 1)^{1/2}, \tag{18}$$

where

$$Y = |y|^2 + |y^2 - 1|, \quad y = y_r + iy_i. \tag{19}$$

The imaginary part of the parameter y is determined by the absorption. If the absorption is negligible then the total reflection takes place in the region of $|y_r| < 1$. According to equation (13) the angular width of the total reflection region is determined by the equation

$$|\Delta\theta| < \frac{|D_1|}{\sin(2\theta_B)}\frac{1}{|\Delta\varphi|}. \tag{20}$$

It depends on the deviation of the azimuthal angle from the exact multiple diffraction condition. Interestingly, this dependence is slower compared to the reflection power of beam 2, which is proportional to $|\Delta\varphi|^{-2}$.

In the center of the angular region of total reflection we have $y_r = 0$, $Y = 1 + 2y_i^2$, $\widetilde{R}_1 \simeq Y - 2y_i$ for small values of y_i. For large values of $|\Delta\varphi|$ we have an approximate expression for the parameter y_i as $y_i = \mu_0 L_{ex}/2\gamma_0$, where $\mu_0 = 2\pi\chi_{0i}/\lambda$ is a linear absorption coefficient, $L_{ex} = 2/\Re(-g_{01}g_{10})^{1/2}$ is an extinction length. Therefore y_i describes the absorption on the extinction length. Since L_{ex} becomes very large for the large azimuthal angles the total reflection cannot be realized for all azimuthal angles. For example, $\widetilde{R}_1 = 0.5$ for $Y = 1.25$ and $y_i = 0.35$.

Inside the total reflection region the maximum value of the reflection power corresponds to the angle where y_i is minimal. From equation (13) we can write approximately

$$y_i = \frac{\chi_{0i} + y_r|X_{1i}|}{X_{1r}}. \tag{21}$$

In the normal two-beam case $|X_{1i}|$ is comparable with χ_{0i}, and in the left part of the total reflection region at $y_r = -1$ a significant decrease in the value of y_i takes place and this is the reason for the Borrmann anomalous transmission phenomenon. However, in our case $|X_{1i}|$ is much smaller than χ_{0i}; therefore the Borrmann effect is not observed.

Table 1
The estimated values of the energy and angular resolution for the experimental setups in Fig. 1.

	Setup 1	Setup 2	Setup 3	Setup 4	Setup 5
$\Delta\lambda/\lambda$ (10^{-6})	290	25.6	3.6	25.6	3.6
$\Delta\theta_V$ (μrad)	23	4.7	1.4	4.7	1.4
$\Delta\theta_H$ (μrad)	115	115	115	7.6	7.6

There is an interesting peculiarity of the reflection into the second reflection if the Bragg condition (including refraction) is fulfilled completely for the first (forbidden) reflection. Indeed, the set of equations (2) without polarizations can be written as

$$\begin{pmatrix} G_{00} & 0 & G_{02} \\ 0 & G_{11} & G_{12} \\ G_{20} & G_{21} & G_{22} \end{pmatrix} \begin{pmatrix} B_0 \\ B_1 \\ B_2 \end{pmatrix} = \varepsilon \begin{pmatrix} B_0 \\ B_1 \\ B_2 \end{pmatrix}. \qquad (22)$$

The Bragg condition for the first reflection reads $G_{11} = G_{00}$. One can verify straightforwardly that in this case the system has a solution with $B_2 = 0$, $\varepsilon = G_{00}$, $B_1 = -G_{20}B_0/G_{01}$. This solution is independent of the azimuthal angle, *i.e.* even in the exact multiple diffraction region the reflection into a second beam vanishes. In reality we can satisfy the condition only for the real parts $\Re(G_{11}) = \Re(G_{00})$ if $\Delta\theta = -\Re(\chi_0)/\sin(2\theta_B)$. The imaginary parts do not satisfy this condition; therefore the reflection into the forbidden beam vanishes for very large values of the azimuthal angle. Nevertheless, the phenomenon of vanishing of the reflection into the second beam inside the multiple diffraction region seems to be rather interesting.

3. Experiment

The experiment was performed at the Cornell High Energy Synchrotron Source (CHESS) at the A2 beamline. The X-ray beam from the 49-pole wiggler was monochromated to an energy of 24.982 keV by a double-crystal Si 111 upstream water-cooled monochromator. Post-monochromator optics for additional monochromatization and angular collimation were assembled on the optical table in the experimental hutch. The sample, an Si (111)-oriented thick perfect crystal, was mounted on a four-circle diffractometer. The diffraction plane for the forbidden 222 reflection was vertical. The 222 and 113 diffracted intensities were recorded as a function of the polar angle θ for various values of the azimuthal angle φ. The 222 intensity was normalized to the intensity of the incident beam recorded by the intensity monitor installed in front of the sample.

The optical arrangements are shown schematically in Fig. 1. Two diffraction planes, vertical (V) and horizontal (H), are shown for each setup. The values for the energy bandwidth and the angular collimation characteristic for each setup are summarized in Table 1. Experimental diffraction curves measured by using each setup are compiled in Fig. 2 (note different angular and intensity scales). Each column in Fig. 2 contains diffraction data obtained by using a particular optical setup.

We start with a 'standard' beamline setup in which the energy bandwidth and the angular collimation are determined by the double-crystal Si 111 monochromator, the source size and the slits. With a wiggler source size of 0.38 (vertical) × 3.38 mm (horizontal), a size of the S3 slit in front of the sample of 0.5 × 1 mm and a distance between the source and the slit

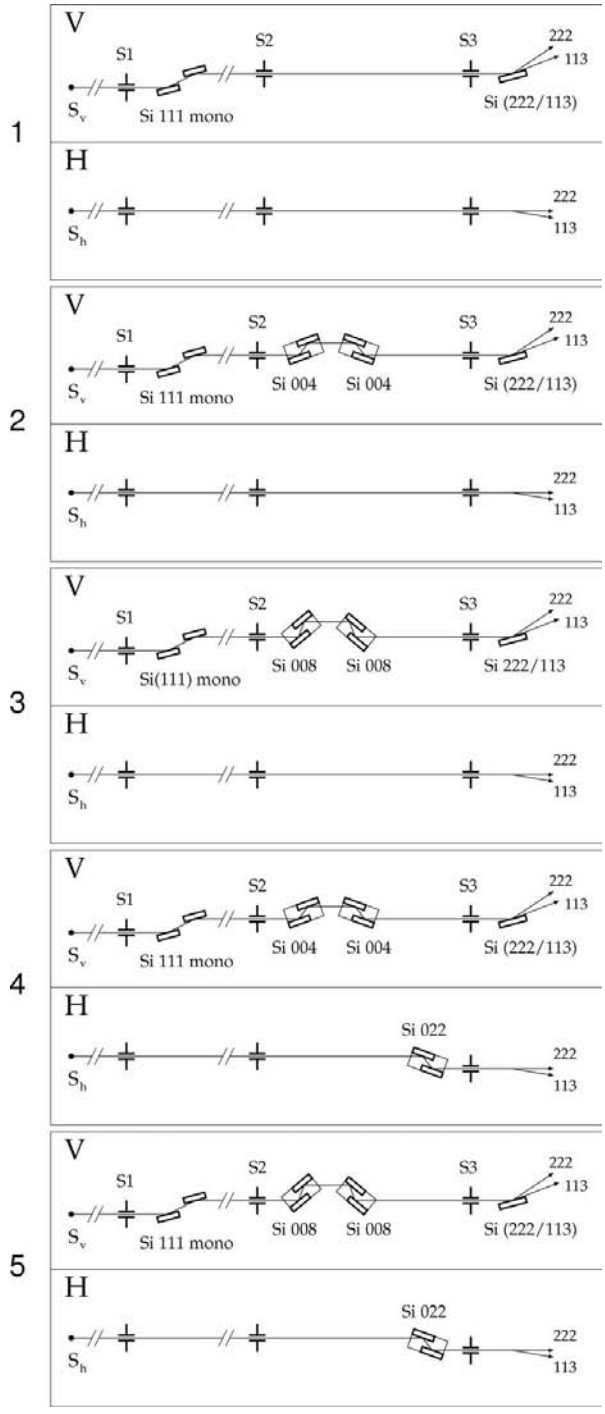

Figure 1
Experimental setups are indicated by the numbers shown on the left. Each setup is shown by two panels: one, marked by 'V', is in the vertical plane (diffraction plane for the 222 reflection) and the other one, marked by 'H', is in the horizontal plane.

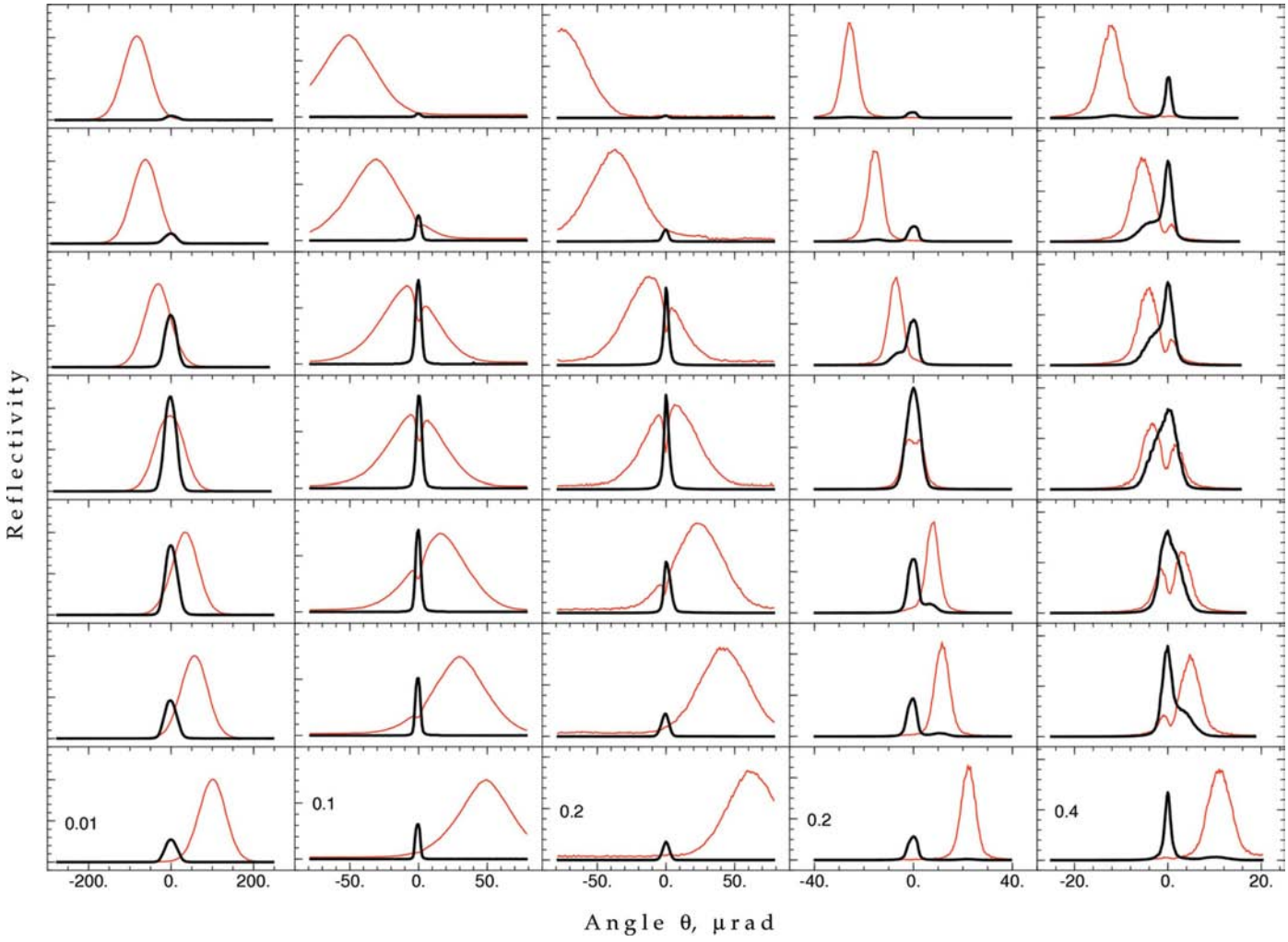

Figure 2
The 222 (thick black lines) and 113 (thin red lines) diffraction curves measured using the experimental setups shown in Fig. 1. The 222 curve is normalized on the incident intensity. Setup 1 (first column): the azimuthal angle φ, from top to bottom: 86, 63, 31, 1.0, −35, −59 and −101 μrad; setup 2: 90, 53, 12, 2.7, −28, −53 and −88 μrad; setup 3: 134, 65, 21, −9, −39, −74 and −109 μrad; setup 4: 45.5, 27.6, 12.9, 0, −7.7, −21.8 and −38.8 μrad; setup 5: 21.6, 9.5, 5.1, 1.9, −2.2, −8.5 and −19.4 μrad.

of 38 m, we estimate the angular collimation in the vertical plane as 23 μrad and in the horizontal plane as about 115 μrad. (These values are smaller than the angular spread of the wiggler radiation of 150 μrad in the vertical and 285 μrad in the horizontal plane.) The estimated energy bandwidth $\Delta E/E$ is 2.9×10^{-4}, close to the experimentally measured value of 3.0×10^{-4}. The experimental curves (first column in Fig. 2) are much narrower for the 222 reflection than for the 113 reflection because the 222 reflection does not depend on the azimuthal angle φ whereas for the 113 reflection the region of the strong reflection projected on the θ axis shifts with changing φ. The enhancement of the 222 peak in the center of the three-beam region is clearly seen with the maximum 222 reflectivity of about 2%. Any dynamical effects described in the previous sections are washed out by the angular spread of the incident beam.

In all other optical schemes two double-bounce channel-cut crystals in the antiparallel (+/+) setting were used to obtain a higher degree of monochromatization and improve the angular collimation in the vertical plane: Si 004 in setups 2 and 4, and Si 008 in setups 3 and 5 (Fig. 1). For the antiparallel setting both the energy bandwidth and the angular spread are determined by the intrinsic rocking-curve width $\omega_{\rm in}$ of the crystals: $\Delta\lambda/\lambda = \omega_{\rm in}/\tan(\theta_{\rm B})$ and $\Delta\theta_{\rm V} = \omega_{\rm in}$. The calculated values are 2.56×10^{-5} and 4.7 μrad for setups 2 and 4, and 3.6×10^{-6} and 1.4 μrad for setups 3 and 5. As one can see by comparing the results shown in the first three columns in Fig. 2, the additional collimation/monochromatization has a strong effect on the 222 reflection: the reflectivity of 36% was measured using setup 3.

These improvements do not affect the width of the 113 curves but lead to a sharp intensity drop in the angular range of the 222 reflection. To improve the angular collimation in the other direction an additional Si 022 channel-cut crystal diffracting in the horizontal plane was installed (setups 4 and 5). The width of the 113 reflection changes from about 80 μrad for setup 1 to 6.8 μrad for setup 4. The best two-dimensional collimation and monochromatization were achieved with

setup 5, which resulted in the maximum 222 reflectivity of 68%. The experimental width of the 222 curve off the three-beam condition was 1.2 μrad. The deep minimum in the 113 intensity is observed in the central three-beam diffraction region for the angular interval of the 222 reflection. According to the theory presented in the previous section, for a perfect incident plane wave the 113 intensity should be zero for the exact 222 diffraction condition. This effect may serve as an indicator of the quality of the plane-wave optics. The azimuthal dependence of the maximum reflectivity (thick black line) and the integral intensity (thin red line) of the 222 reflection measured using setup 5 are shown in Fig. 3. Both curves show a strong φ asymmetry.

To quantify independently setup 5, after the three-beam measurements were complete the sample was turned off the three-beam condition and was used as an analyzer crystal. The Si 111, 333 and 555 analyzer curves are shown in Fig. 4 (lower panel). The 111 curve shows a perfect Darwin curve with the reflectivity very close to 100%. The 333 reflectivity is 86% and the full width at half maximum is 2.9 μrad *versus* 99% and 1.97 μrad for the theoretical 'intrinsic' curve. The 555 analyzer curve gives 40% reflectivity and 1.68 μrad width *versus* 97.5% and 0.84 μrad for the 'intrinsic' curve. The later results confirm that the beam produced with our best setup is far from being a perfect plane wave. Two 222 curves are shown in the upper panel of Fig. 4. The thick black line is the 222 curve in the center of the three-beam diffraction region; its width is close to the width of the 113 reflection. The 222 curve measured at the $\Delta\varphi$ = 10 μrad off the exact three-beam condition is shown as a thin (red) line. Note that the width of this curve is close to the width of the 555 analyzer curve, indicating that they are both limited by the resolution of our setup. A remarkable effect which has never been observed before is clearly demonstrated: the width of the 222 curve can be changed several times (about four times with these optics) by tuning the azimuthal angle by only a few μrad. This effect can be used for tuning the energy resolution of monochromators based on multiple diffraction.

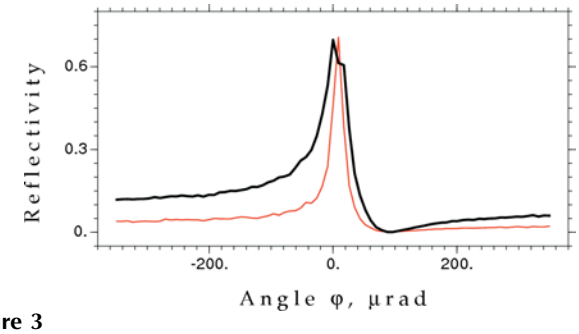

Figure 3
Azimuthal (φ) dependences of the absolute reflectivity (thick black line, left scale) and the intensity integrated over the polar angle θ (thin red line, arbitrary units) of the 222 reflection.

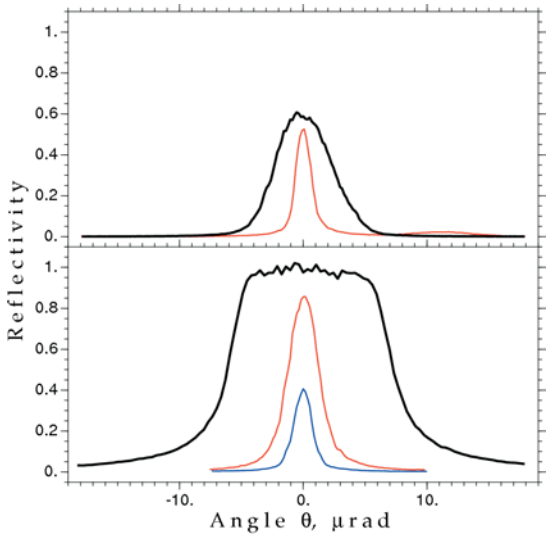

Figure 4
Top: the 222 reflectivity (thick black line) corresponds to the center of the three-beam diffraction region, the thin red line corresponds to the angle $\Delta\varphi$ = 10 μrad off the exact three-beam condition. Bottom: the analyzer 111 (black), 333 (red) and 555 (blue) curves measured with the beam prepared with setup 5.

4. Discussion

The analysis of the experimental results assembled in Fig. 2 led us to the conclusion that improving the angular collimation in the horizontal plane results in narrowing the θ width of the 113 diffraction curves (compare setups 2, 4, 3 and 5), and it also affects the 222 reflection inside the 'intrinsic' three-beam region. On the other hand, better monochromatization and angular collimation in the vertical plane lead to narrower 222 curves outside the three-beam region, and, finally, to the observation of the fine structure in both 222 and 113 reflections in setup 5. This is remarkably different from the two-beam diffraction curves usually measured in a non-dispersive setup when the spreads in energy and in the azimuthal angle do not affect the curves. The 222 reflection curves outside the three-beam case still depend on the azimuthal angle because of the virtual three-beam diffraction, though this dependence is slow. As for the 113 reflection, as one can see in §2, both angles, θ and φ, as well as the energy, enter the formula in equation (4), which describes the deviation from the exact three-beam condition, in a very similar way.

To compare experimental results with theory, the 222 and 113 diffraction curves were calculated for approximately the same values of the azimuthal angle φ as for the experimental curves in Fig. 2 (last column, setup 5). They are shown in Fig. 5. Calculations for the perfect plane wave are in the left panel. The 222 curves show 100% reflectivity and their shape clearly demonstrates two excitation mechanisms as described in §2. The first one corresponds to the 'pumping' of the strong 113 intensity into the 222 beam; it results in the peak with the angular position which corresponds to the 113 reflection. The second, a narrower peak, is excited resonantly and its center angular position corresponds to the Bragg condition for the 222 reflection. At this angle the 113 beam has zero intensity; therefore the total region of reflection splits into two peaks.

The effect of the finite angular and energy resolution on the diffraction curves can be taken into account based on equation

(4). The change in energy is equivalent to the angular shift in θ of both 222 and 113 curves. It was found that for the experimental value of $\Delta\lambda/\lambda$ the effect of the finite monochromaticity is negligibly small. To account for the finite angular spread the 222 and 113 curves were summed over the angular interval $\Delta\varphi = 8$ µrad and the result was convoluted with a Gaussian function with width $\Delta\theta = 1$ µrad. The resulting curves are shown in the right panel in Fig. 5. As one can see, they reproduce the experimental curves remarkably well. We may conclude that although the achieved resolution was sufficient to observe the effects predicted by theory, a better angular resolution in both vertical and horizontal planes is required for a detailed quantitative comparison with theory.

The theoretical treatment (§2) assumed a purely forbidden reflection. This is not the case for Si 222. It is well known that the 222 reflection is very weak but not completely forbidden (Bragg, 1921) due (mostly) to the non-spherical valence charge density (Roberto & Batterman, 1970; Colella, 1977). In our experiment it can be seen in two ways (see Fig. 3): first, the intensity of the 222 beam is approaching a nonzero value as the crystal is rotated far from the three-beam condition; secondly, the strong asymmetry of the φ dependence clearly indicates the phase of the structure factor. Most of the experimental measurements of the structure factors for forbidden reflections were performed by measuring the intensity integrated over the polar angle θ (see *e.g.* Roberto & Batterman, 1970). Accurate rocking-curve measurements in a double-crystal 222 nondispersive (+/−) setup were performed by Entin & Smirnova (1989). They reported a width of the double-crystal rocking curve measured with Mo $K\alpha$ radiation of 0.339 µrad, which was consistent with the structure factor $F_{222} = 1.47$ reported by others. This value gives us an estimate of the intrinsic Si 222 width for our energy as 0.13 µrad. The experimental data presented in Fig. 3 can be used for the determination of both the modulus and the phase of the structure factor.

A high degree of two-dimensional collimation was achieved in this work by using perfect crystal optics. This resulted in a loss of intensity by many orders of magnitude. Next-generation synchrotron sources such as the ERLs (Gruner & Bilderback, 2003) and the XFELs (Pellegrini & Stöhr, 2003) are characterized by extremely high brilliance and produce highly parallel X-ray beams. For such sources the requirements for two-dimensional collimation can be easily fulfilled without significant loss in flux, thus making X-ray optics based on multi-beam diffraction effects extremely attractive.

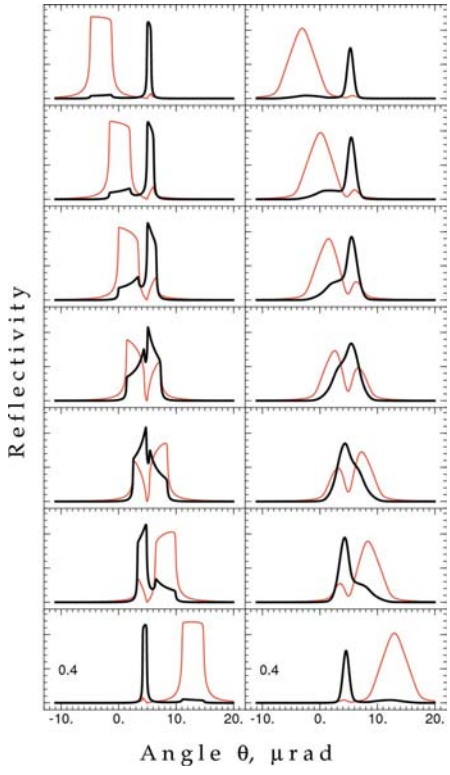

Figure 5
Theoretical diffraction curves 222 (thick black line) and 113 (thin red line) calculated for the perfect plane wave (left) and taking into account the energy and the angular resolution of the experimental setup (right). The values of the azimuthal angle from bottom to top are: −13.5, −4.5, −1.5, 1.5, 4.5, 7.5, 13.5 µrad. The zero point at the angle axis corresponds to the kinematical Bragg angle.

This work is based upon research conducted at the Cornell High Energy Synchrotron Source (CHESS), which is supported by the National Science Foundation and the National Institutes of Health/National Institute of General Medical Sciences under NSF award No. DMR-0225180. The work of V. G. Kohn was supported by RFBR grant Nos. 09-02-12164-Ofi_m and RS-4110.2008.2.

References

Afanas'ev, A. M. & Kohn, V. G. (1977). *Acta Cryst.* A**33**, 178–184.
Authier, A. (2005). *Dynamical Theory of X-ray Diffraction*, 3rd ed. Oxford University Press.
Bragg, W. H. (1921). *Proc. Phys. Soc. London*, **33**, 304–311.
Chang, S.-L. (2004). *X-ray Multiple-Wave Diffraction: Theory and Application*, Springer Series in Solid-State Sciences. Berlin: Springer.
Colella, R. (1974). *Acta Cryst.* A**30**, 413–423.
Colella, R. (1977). *Phys. Scr.* **15**, 143–146.
Entin, I. R. & Smirnova, I. A. (1989). *Acta Cryst.* A**45**, 577–580.
Gruner, S. M. & Bilderback, D. H. (2003). *Nucl. Instrum. Methods Phys. Res. Sect. A*, **500**, 25–32.
Høier, R. & Marthinsen, K. (1983). *Acta Cryst.* A**39**, 854–860.
Kazimirov, A. Y., Kovalchuk, M. V., Kharitonov, I. Y., Samoilova, L. V., Ishikawa, T. & Kikuta, S. (1992). *Rev. Sci. Instrum.* **63**, 1019–1022.
Kazimirov, A. Y., Kovalchuk, M. V., Kohn, V. G., Ishikawa, T., Kikuta, S. & Hirano, K. (1993). *Europhys. Lett.* **24**, 211–216.
Kazimirov, A. Y., Kovalchuk, M. V., Kohn, V. G., Kharitonov, I. Y., Samoilova, L. V., Ishikawa, T., Kikuta, S. & Hirano, K. (1993). *Phys. Status Solidi A*, **135**, 507–512.
Kohn, V. G. (1979). *Phys. Status Solidi*, **54**, 375–384.
Kohn, V. G. (1988). *Kristallografiya*, **33**, 567–573.
Pahl, R. (1994). *Nucl. Instrum. Methods Phys. Res. Sect. A*, **347**, 491–494.
Pellegrini, C. & Stöhr, J. (2003). *Nucl. Instrum. Methods Phys. Res. Sect. A*, **500**, 33–40.
Roberto, J. B. & Batterman, B. W. (1970). *Phys. Rev. B*, **2**, 3220–3226.
Stepanov, S. A., Kondrashkina, E. A., Novikov, D. V. & Imamov, R. M. (1994). *Nucl. Instrum. Methods Phys. Res. Sect. A*, **346**, 385–393.